J. Fluid Mech. (2001), *vol.* 439, *pp.* 87–108. Printed in the United Kingdom

On the orbital response of a rotating cylinder in a current

By P. K. STANSBY[1] AND R. C. T. RAINEY[2]

[1]Department of Civil and Construction Engineering, UMIST, Manchester M60 1QD, UK

[2]Centre for Nonlinear Dynamics, University College London, Gower Street, London WC1E 6BT, UK; also W. S. Atkins Consultants Ltd, Ashley Road, Epsom, Surrey KT18 5BW, UK

(Received 8 March 2000 and in revised form 15 December 2000)

A new form of dynamic response has been observed in some simple experiments with a lightly damped rotating cylinder in a current. The response is orbital with a period several times the structural natural period and an amplitude ranging up to many diameters. It is mainly dependent on the ratio of current velocity to cylinder surface velocity, α, and the reduced velocity, V_r (the ratio of current velocity to the product of natural frequency in water and diameter). Big orbital responses occur with $0.25 < \alpha < 0.5$ and $V_r > 5$, and are accompanied by the expected large static response. To understand the flow mechanisms causing this response computational simulations have been made for two-dimensional laminar flow and the experimental response characteristics are qualitatively reproduced. Streamline and vorticity contour plots are output through a cycle and are related to instantaneous values of lift and drag coefficients and α (all based on flow relative to the cylinder). The movement of the stagnation point away from and towards the cylinder surface with intermittent wake formation in a cycle causes a large lift variation which is mainly responsible for the dynamic response. The variation of lift coefficient with α (as defined above) shows a generally negative gradient, and a pronounced hysteresis loop when substantial response occurs for $\alpha \gtrsim 0.25$. The computations show that a small-amplitude, high-frequency response may also be superimposed on the high-amplitude, low-frequency response, most noticeably for $\alpha \lesssim 0.25$. This is consistent with a simple potential-flow idealization of the lift force. For $\alpha \sim 0.2$ a large dynamic response, not observed in the experiments, was produced in the computations due essentially to attached boundary-layer behaviour.

1. Introduction

For deep-water offshore oil exploration the possibility of using a drillstring without an outer casing is of operational interest. It poses the hydrodynamic problem of a flexibly mounted rotating cylinder in a current, which has not previously been investigated to the authors' knowledge, and is of fundamental interest.

Elementary theoretical considerations are first addressed, in §2. It is shown that the effect of the rotation of the cylinder is to produce two new circular modes of vibration, one at a higher frequency than the previous natural frequency of vibration, and one at a lower. Whether either can be self-exciting in a current will depend on non-elementary (i.e. non-potential-flow) considerations. These are first discussed in §3 for the simpler case of a non-responding (fixed-axis) cylinder, using two-

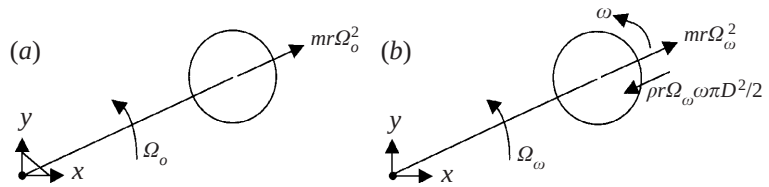

FIGURE 1. Forces on a cylinder moving in a circular orbit: (*a*) non-rotating, (*b*) rotating.

dimensional laminar flow computations, which are compared with published results. Experimental results with a responding cylinder are then presented in § 4, and the cases of large self-excited response are highlighted. In § 5 our two-dimensional laminar-flow computations for the responding case are compared with the experimental results and in § 6 corresponding force and flow characteristics are discussed.

2. Elementary theoretical considerations

The motions of a cylinder in two dimensions, with circulation, is concisely treated in Milne-Thomson (1968, § 9.24), using complex variables. That treatment could be simply extended to cover the present case in which the cylinder is effectively constrained by a spring. From a physical point of view, however, it is more instructive to consider the balance of radial forces during orbital motion (i.e. motion with the cylinder behaving like a skipping rope).

Consider first the case when the cylinder is not rotating, so that there is no circulation around it, at least initially. As the cylinder executes a circular orbit about its rest position, with angular frequency Ω_o and radius r, the centrifugal force shown in figure 1(*a*) will be balanced by the spring stiffness, thus

$$mr\Omega_o^2 = kr,$$

giving

$$\Omega_o = \sqrt{k/m} = \sqrt{k/[(1+\beta)\rho\pi D^2/4]}, \tag{1}$$

where m is the mass and added mass, which is, assuming potential flow, $(1+\beta)\rho\pi D^2/4$, ρ is the density of the fluid, $\beta\rho$ the density of the cylinder, D is its diameter, k is the restoring stiffness; m and k are per unit length of cylinder. There is a similar circular mode in the other direction, and an arbitrary elliptical motion can be synthesized by a suitable linear combination of these two modes, in the appropriate phase.

The advantage of these circular modes over the conventional rectilinear modes in the x- and y-directions shown (which arise as solutions of the conventional equations of motion in those coordinates, see (6) and (7) below) can be seen when we consider a cylinder which is rotating (at an angular frequency ω, say). If we assume a zero-slip condition at the cylinder surface, then the potential flow around it will have a circulation $\omega\pi D^2/2$ (we can more generally allow for an arbitrary circulation simply by replacing ω by $c_L\omega$, given the definition of c_L later in this paper). Thus if the circular mode now has angular frequency Ω_ω, in the same sense as ω, the lift force will be $\rho r\Omega_\omega\omega\pi D^2/2$ (see for example Batchelor (1967), equation 6.4.26) as shown in figure 1(*b*). Thus the equilibrium of radial forces now gives

$$mr\Omega_\omega^2 = kr + \rho r\Omega_\omega\omega\pi D^2/2,$$

giving

$$\left.\begin{aligned}\Omega_\omega^2 - 2\Omega_\omega(\rho\omega\pi D^2/4)/[(1+\beta)\rho\pi D^2/4] - \Omega_o^2 = 0,\\ \Omega_\omega^2 - 2[R/(1+\beta)]\Omega_o\Omega_\omega - \Omega_o^2 = 0,\end{aligned}\right\} \tag{2}$$

where $R = \omega/\Omega_o$ is the ratio of the angular rotational speed of the cylinder to the angular orbital speed of vibration (i.e. the angular frequency of vibration) of the non-rotating cylinder. (Again, if we wish to allow for arbitrary circulation around the cylinder, we can replace R with $c_L R$.) We can readily solve the quadratic equation as

$$\Omega_\omega = \Omega_o(R/(1+\beta) \pm \sqrt{R^2/(1+\beta)^2 + 1}) \tag{3}$$

so the original circular modes of angular frequency Ω_o in either direction become a circular mode of higher angular frequency than Ω_o in the same sense as ω, and one with a lower angular frequency than Ω_o in the opposite sense to ω. When the parameter $R/(1+\beta)$ is large, we can write

$$\begin{aligned}\Omega_\omega &\simeq \Omega_o[R/(1+\beta)](1 \pm (1 + [R/(1+\beta)]^{-2}/2))\\ &\simeq \Omega_o[2R/(1+\beta)] \quad \text{or} \quad -\Omega_o/[2R/(1+\beta)].\end{aligned} \tag{4}$$

It is the latter mode, with the cylinder orbiting slowly in the opposite sense to its rotation, with stiffness and lift forces almost cancelling, that will particularly concern us.

We will also wish to consider the effect of a current of velocity V, say. For consistency with earlier work on non-responding (fixed-axis) cylinders, we non-dimensionalize by the surface velocity on the cylinder $\omega D/2$, and write $\alpha = V/(\omega D/2)$. Also for consistency with earlier work on flexibly mounted cylinders, we use the conventional 'reduced velocity' $V_r = 2\pi V/(\Omega_o D)$. Thus we can express our parameter R above as $R = \omega/\Omega_o = V_r/(\pi\alpha)$.

Since we can write the potential-flow lift force in vector notation as

$$\rho\Gamma \boldsymbol{i} \times (\boldsymbol{V} - \boldsymbol{v}) = \rho\Gamma \boldsymbol{i} \times \boldsymbol{V} - \rho\Gamma \boldsymbol{i} \times \boldsymbol{v}, \tag{5}$$

where Γ is the circulation, $\boldsymbol{i}$ is a unit vector along the cylinder axis, $\boldsymbol{V}$ is the current velocity vector and $\boldsymbol{v}$ is the cylinder velocity, we can see that the effect of the current is simply to produce an additional steady lift force, which is independent of the cylinder velocity. Thus with potential flow, a current should simply produce a steady sideways (i.e. cross-current) offset of the cylinder, without affecting the orbital motion discussed above.

The final elementary consideration is the mechanical damping on the cylinder. It is well known from the theory of whirling shafts that this can be either 'external' or 'internal' (see Bishop 1959, equation 40). Both give a symmetric contribution to the damping matrix (i.e. a dissipative contribution in contrast to the lift force considered in figure 1(*b*) which gives a skew-symmetric contribution to the damping matrix, which does not dissipate energy), but the latter also gives a skew-symmetric (i.e. destabilizing) contribution to the stiffness matrix (see (6) and (7) below).

The effective damping produced by non-potential-flow effects in the fluid is addressed in the remainder of this paper. We should remark that the nonlinearities in this effective damping are in principle likely to give rise to complex dynamic phenomena in certain cases, such as co-existing limit cycles, and even chaotic motion. The simpler case of unimodal galloping is discussed in Thompson & Stewart (1986, § 4.4), and Thompson (1982) describes a bimodal flutter more analogous to the present case. It is not, however, the purpose of the present paper to explore these interesting

phenomena. Rather, we have made an initial investigation of the problem only, by means of a relatively limited series of experiments and computations.

3. Non-responding rotating cylinder

This flow has received much attention over the years (from Betz 1925 and Prandtl & Tietjens 1934) and is defined by $\alpha = U_{cur}/U_{rot}$ and a Reynolds number, usually $Re_{cur} = U_{cur}D/\nu$ where U_{cur} is the current velocity, U_{rot} is the cylinder surface velocity, D is cylinder diameter and ν is the kinematic viscosity of water.

A computational study has been made with $Re_{cur} = 10^3$ by Chew, Cheng & Luo (1995), based on the vortex method. In this study the finite-volume method of Lien & Leschziner (1994) for unsteady flow with second-order-accurate advection has been modified for two-dimensional flow around a cylinder. A polar mesh is used with periodic boundary conditions in the angular direction and exponential stretching in the radial direction, giving refinement near the surface to resolve boundary-layer behaviour. Such a mesh was previously used by Smith & Stansby (1988) for the vortex method. For this application cylinder rotation has been incorporated by specifying the cylinder surface velocity and, at the outer boundary, by adding the velocity due a bound potential vortex to the incident flow velocity. (The influence of the bound vortex had little effect possibly because the outer boundary was at a radius of at least $20D$ from the centre.)

In order to investigate the fundamental nature of these flows through computational simulation, laminar conditions are chosen where computation is known to be accurate. (Turbulence modelling is notoriously difficult in wake regions and three-dimensional direct numerical simulation is not yet a practical computing proposition.) Here meshes with 80×80 and 120×120 cells with an inner radial mesh spacing of $\sqrt{2\nu\Delta t}$ (the diffusion length scale), where Δt is the time step, gave force variations with time which were identical almost to within plotting accuracy. Figure 2 shows streamline plots with $Re_{cur} = 200$ and $\alpha = 0.2$, 0.25, 0.3, 0.5 and 1.0. This is approximately the highest Reynolds number for which the flow is expected to be two dimensional and laminar according to the theoretical analysis of Karniadakis & Triantafyllou (1992) (for a non-rotating cylinder). For $\alpha = 0.2$ the stagnation point is detached from the cylinder surface (and on the y-axis); the streamlines are similar to those of a point vortex in a uniform stream. For $\alpha = 0.25$ the stagnation point has moved closer the cylinder surface and a steady wake has started to form with $\alpha = 0.3$. Note that the stagnation point never actually reaches the surface due to the surface velocity. For $\alpha = 0.5$ the wake has increased in size but remains attached, fluctuating slightly about a mean position. For $\alpha = 1$ vortex shedding has become established, generating fluctuating lift and drag forces as shown in figure 2(f). Note here that the drag fluctuation is at the same frequency as the lift, in contrast to the well-known case without rotation where the drag frequency is twice that of the lift. The dependence of these flows on α is consistent with the early experimental visualizations shown in Prandtl & Tietjens (1934).

Computed variations of mean lift and drag with α are shown in figure 3 with $Re_{cur} = 200$ and 10^3 (the latter for comparison with the results of Chew *et al.* 1995),

FIGURE 2. Computed streamline plots for a non-responding rotating cylinder with $Re_{cur} = 200$: (a) $\alpha = 0.2$, (b) $\alpha = 0.25$, (c) $\alpha = 0.3$, (d) $\alpha = 0.5$, (e) $\alpha = 1.0$; (f) lift and drag force variation with time for $\alpha = 1.0$ (force normalized by $\rho U_{rot}^2 D/2$). Flow is from left to right.

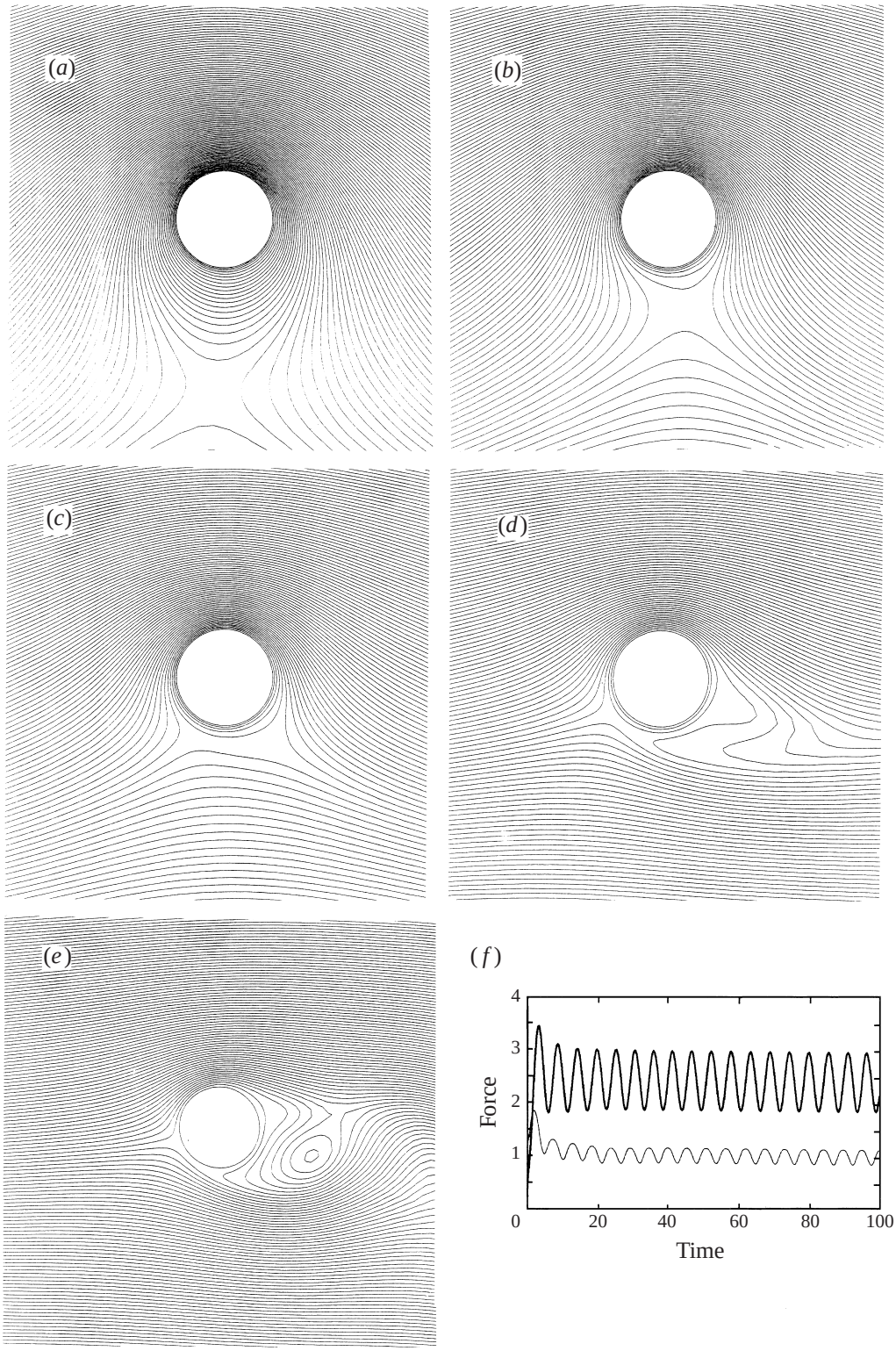

FIGURE 2. For caption see facing page.

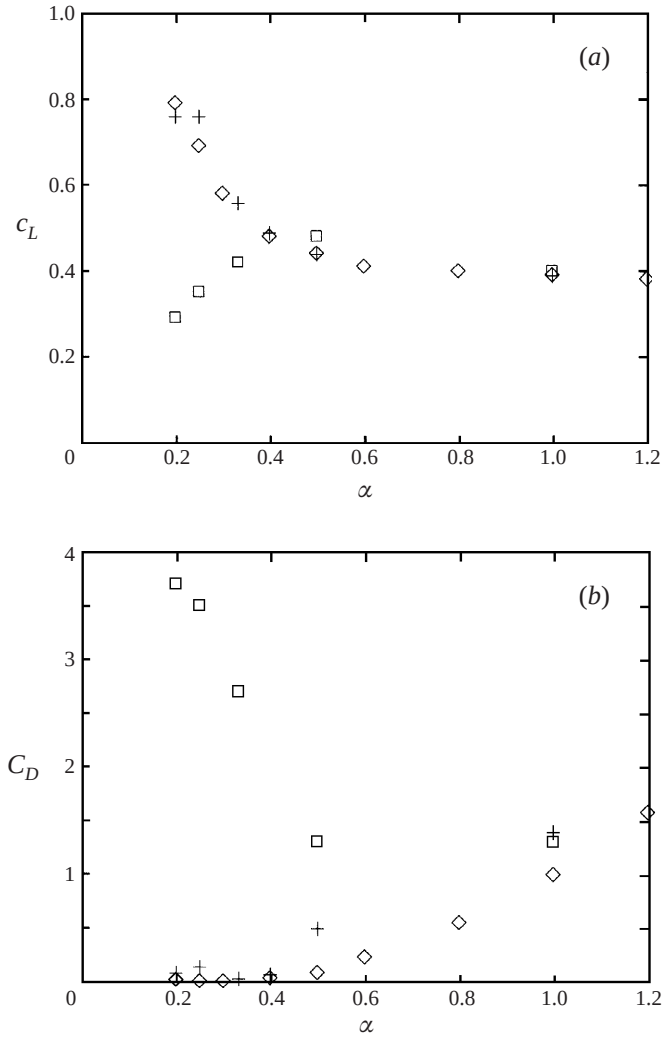

FIGURE 3. Computed mean force coefficients for a fixed rotating cylinder. (*a*) c_L and (*b*) C_D variation with α; ◇, $Re_{cur} = 200$; +, $Re_{cur} = 10^3$; □, Chew *et al.* (1995), $Re_{cur} = 10^3$.

where the drag coefficient is defined in the usual way, $C_D = \text{drag}/(0.5\rho U_{cur}^2 D)$, and lift coefficient is defined as the fraction of the inviscid Magnus force, $c_L = \text{lift}/(\rho U_{cur}\Gamma)$ where $\Gamma = \pi D U_{rot}$. From the present computations, for small α, C_D is very small and $c_L \to 1$ as $\alpha \to 0$ in agreement with the theoretical (asymptotic) analysis of Moore (1957). This is in marked contrast to the results of Chew *et al.* (1995) for the lower α values.

$Re_{cur} = 200$ is also chosen to investigate dynamic response.

4. Experiments with dynamic response

4.1. *Experimental rig*

The cylinder was allowed to respond dynamically with a known mode shape. To achieve this a rigid aluminium cylinder was supported by a thin (2 mm diameter) wire,

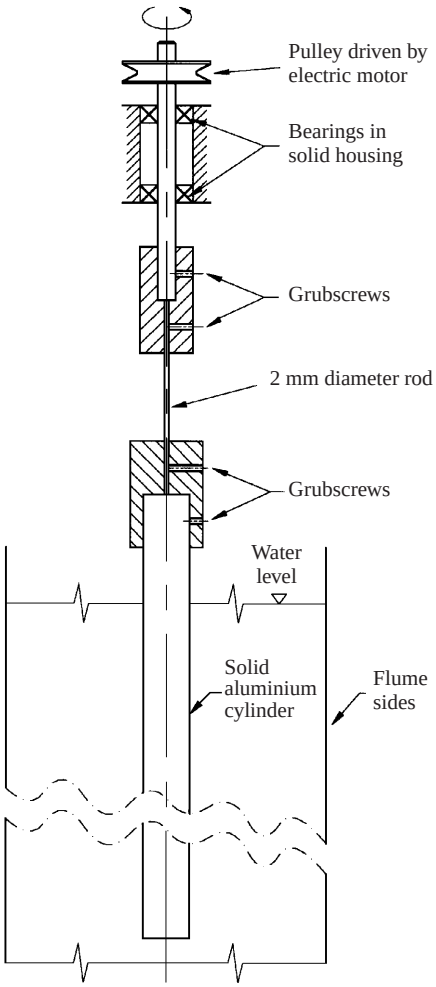

FIGURE 4. Sketch showing cylinder rotation apparatus.

with its axis concentric with that of the cylinder, and forced to rotate by a variable low-speed electric motor. A sketch is shown in figure 4. The density of aluminium of $2720\,\mathrm{kg\,m^{-3}}$ is close to values of practical interest. Cylinders of 12.7 mm and 25.4 mm diameter were used, both of 1.02 m length. Damping tests were conducted in air and water giving the logarithmic decrement δ. In air the damping due to viscosity is negligible and δ is effectively due to internal damping, values between 0.009 and 0.01 being obtained. In water this is not the case as hydrodynamic damping is significant, but the natural frequency is obtained.

A steady current flume was used with a $1\,\mathrm{m} \times 1\,\mathrm{m}$ cross-section and a nearly uniform velocity profile, with less than 3% variation in the working section and a turbulence intensity of about 4%. The water depth was always close to 0.75 m. The cylinder is supported on a frame above the flume and the largest response is thus close to the bed. The gap between the bed of the flume and the end of the cylinder (when vertical) was always close to 1 cm. The range of Reynolds number Re_{cur} was between 800 and 4700.

The displacements at the cylinder base are obtained by video analysis with the

movement of the base over a square mesh on the flume bed recorded. Geometric distortions are accounted for in obtaining the actual displacements.

4.2. *Experimental results*

The predominant motion of the cylinder was a slow orbit combined with a steady offset, as described in § 2 above. After the motion had settled down to a steady state, the peak-to-peak amplitudes of the orbit of the cylinder end in the in-line (x) and cross-flow (y) directions were measured, and are given in figure 5, as a function of different values of $\bar{\alpha}$, for different values of V_r. Note that with a responding cylinder $\bar{\alpha}$ is used to define U_{cur}/U_{rot} since α will later be used to define the value based on the instantaneous velocity relative to the cylinder. Results with the 25.4 mm diameter cylinder for $V_r = 10.97$ are broadly similar to those for the 12.7 mm diameter cylinder with $V_r = 9.45$, indicating that end effects (and therefore effects due to aspect ratio) and effects due to differences in Reynolds number do not have a marked influence.

A quite distinct result is the sudden increase in dynamic response as $\bar{\alpha}$ increases, at $\bar{\alpha} = 0.23$–0.26. If V_r is small enough a significant response does not occur. The maximum dynamic response occurs at $\bar{\alpha} = 0.3$–0.4 and this decreases relatively slowly as $\bar{\alpha}$ increases further, becoming small (relatively) at $\bar{\alpha} = 0.5$–0.6.

The response due to vortex shedding (of the kind associated with a Kármán vortex street) which is likely for $\bar{\alpha} > 0.5$ is not considered here. With a non-rotating cylinder such a response is known to occur for $5 < V_r < 10$, approximately, and for the mass and damping values of these experiments responses of 1–2 diameters, peak-to-peak, would be expected, e.g. Govardhan & Williamson (2000) (and have also been observed with the present rig). Responses of similar magnitude have been observed with the rotating cylinder for $\bar{\alpha} \sim 1$ although it is known that the details of the vortex shedding wakes are different as a result of rotation.

Turning to the steady offset of the cylinder, as opposed to its orbital motion, this was defined as the average of the peak excursions. Mean lift and drag coefficients c_L and C_D have been obtained as shown in figure 6, by converting these steady offsets to forces using the known 'effective' stiffness of the cylinder arrangement. This was deduced from the still-water natural periods and includes the effect of the weight of the pendulum partially immersed in water as well as the stiffness of the cylinder support. The added mass coefficient for the small-amplitude motion of a damping test may be assumed to be very close to unity, e.g. Keulegan & Carpenter (1958). Due account is taken of the contributions of the internal mechanical damping to the stiffness matrix, see (6) and (7) below (this means that the in-line response can occur with $C_D = 0$, provided $c_L \neq 0$). Standard modal analysis (e.g. Clough & Penzien 1975) is used with the assumption that force is uniform over the span of the cylinder. Some wind-tunnel (nominally two dimensional) measurements by Betz (1925) for a non-responding cylinder (with $Re_{cur} = 5 \times 10^4$) are also shown, where care had been taken to remove end effects. These coefficients are generally a little greater than those obtained in our experiments where some scatter is apparent. This is particularly noticeable for C_D at smaller α values where the drag force is small in relation to lift. Note that with $V_r = 25.05$ dynamic response is negligible and these results are thus most appropriate for comparison with the Betz experiments, showing closest agreement.

The period of oscillation T is considerably larger than the natural period T_o. Values of T/T_o for the 12.7 mm and 25.4 mm diameter cylinder are shown in figure 7 with the potential-flow formula given by (3) in § 2 above. The value of c_L is given by the least-squares fit in figure 6. The potential-flow formula can be seen to be up to

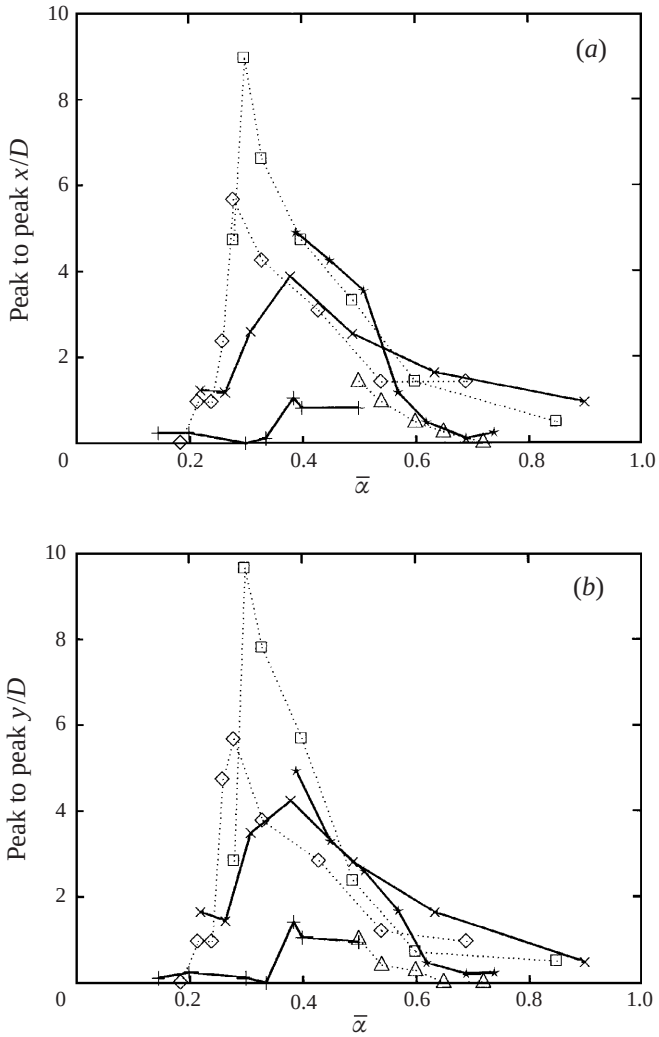

FIGURE 5. Variation of peak-to-peak amplitude with velocity ratio, $\bar{\alpha}$, for the 12.7 mm diameter cylinder: ◇, $V_r = 9.45$; □, $V_r = 14.03$; △, $V_r = 25.05$; and for the 25.4 mm diameter cylinder; +, $V_r = 5.22$; ×, $V_r = 10.97$; *, $V_r = 16.1$. (*a*) In-line response x/D, (*b*) cross-response y/D.

30% less than the experimental measurements while showing similar trends with $\bar{\alpha}$ and V_r.

Since the cylinder is inclined to the vertical while it is orbiting there will inevitably be gyroscopic effects. However the analysis given in the Appendix shows this to be a very small effect.

5. Computed dynamic response

The finite-volume method with cylinder rotation described in § 3 has been extended to include dynamic response. The outer velocity boundary condition now includes the cylinder-axis (translational) velocity as the flow relative to the cylinder is computed; the outer pressure gradient is thus also adjusted to include the effect of cylinder

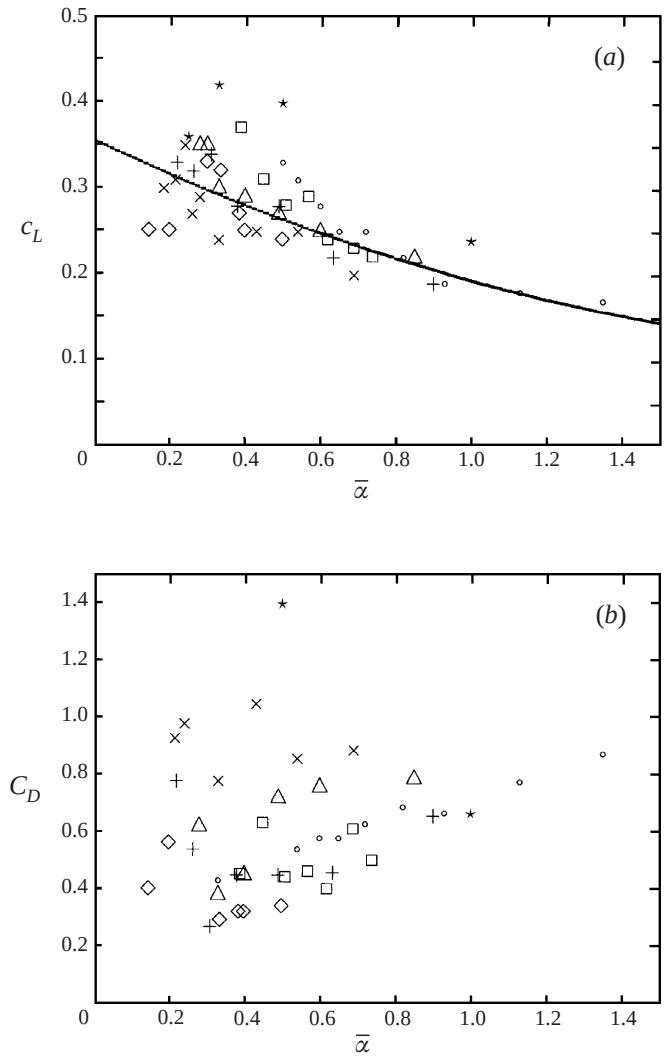

FIGURE 6. (*a*) Mean lift coefficients c_L and (*b*) mean drag coefficients C_D from experiments as a function of $\bar{\alpha}$, using mean response and modal analysis. 25.4 mm cylinder: ◇, $V_r = 5.2$; +, $V_r = 11.0$; □, $V_r = 16.1$; 12.7 mm cylinder: ×, $V_r = 9.5$; △, $V_r = 14.0$; ○, $V_r = 25.05$; *, Betz (1925). The full line is a least-squares fit given by $c_L = 0.355 - 0.204\bar{\alpha} + 0.022\bar{\alpha}^2$ (excluding Betz's results).

acceleration. To obtain the force on the actual responding cylinder the Froude–Krylov force is subtracted from the computed force.

The mass/spring/damper system defining the motion with two degrees of freedom is given, as described in § 2 above, by

$$\ddot{x} + 2c\omega_n\dot{x} + \omega_n^2 x - 2c\omega\omega_n y = F_x/m, \tag{6}$$

$$\ddot{y} + 2c\omega_n\dot{y} + \omega_n^2 y + 2c\omega\omega_n x = F_y/m, \tag{7}$$

where m is now simply the mass per unit length and F_x, F_y are forces per unit length in the x- and y-directions; ω_n and c are *in vacuo*/air values, although the value of natural frequency in water is still used to define V_r.

The experimental situation of the 12.7 mm diameter cylinder with $V_r = 14.03$,

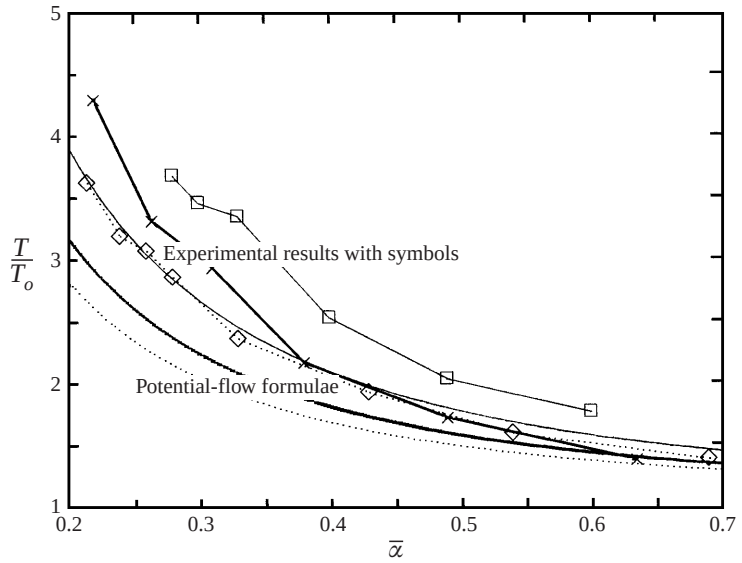

FIGURE 7. The ratio of orbital period to natural oscillation period T/T_o against velocity ratio $\bar{\alpha}$: for the 12.7 mm diameter cylinder: ◇, $V_r = 9.45$; □, $V_r = 14.03$; and for the 25.4 mm diameter cylinder: ×, $V_r = 10.97$. Theoretical curves of T/T_o from (3) are shown with the line type corresponding to those joining the experimental points.

for $\bar{\alpha} = 0.15$, 0.2, 0.25, 0.3, 0.4 and 0.5 and $\delta = 0.01$, is chosen for computation, covering a wide range of responses. In addition, the cases with $\alpha = 0.3$ and 0.5 are repeated with $V_r = 25$, corresponding to another experimental situation with the 12.7 mm diameter cylinder. The orbital nature of the computed response can be seen in the plots of y against x which are given in figure 8. A large response always builds up after the cylinder is released and the dynamic component either decays or reaches a periodic state. The ratios of orbital period to the natural period of oscillation T/T_o corresponding to Figures 8(a)–8(g) are 14.7, 8.8, 6.0, 4.6, 3.3, 2.6 and 6.6 respectively. The ratios according to the potential-flow formula given in (3) are 12.5, 8.9, 6.8, 4.7, 3.1, 2.5, and 8.1, with c_L values from figure 3 and are in approximate agreement with those from the computations. The agreement is somewhat better than the corresponding comparison for experimental results shown in figure 7.

A high-frequency oscillation is also quite evident with $\bar{\alpha} = 0.15$ to 0.5 for V_r=14. According to (3) the ratio of the high-frequency oscillation to the main orbital frequency, corresponding to figures 8(a)–8(f), should be 156, 82, 45, 22, 9.7, 6.3 respectively and basic manual calculation from these figures shows broadly similar values.

Dynamic response with $\bar{\alpha} = 0.5$ decays rapidly for $V_r = 25$ (figure 8h) and rather slowly for $V_r = 14$ (figure 8f). For the latter, dynamic response in the experiments has become small and $\bar{\alpha} = 0.5$ appears to be the upper limit for dynamic response. With $\bar{\alpha} = 0.3$, dynamic response in the x-direction is greater for $V_r = 25$ than for $V_r = 14$ while dynamic response in the y-direction is similar.

The responses are somewhat greater than the experimental results for peak-to-peak amplitudes shown in figure 5, particularly bearing in mind that the experiments show tip response and the computed (uniform-mode) results compare with the mid-depth experimental results (assuming uniform loading). Note, however, that while in the experiment the steady lift force will be uniformly distributed along the cylinder

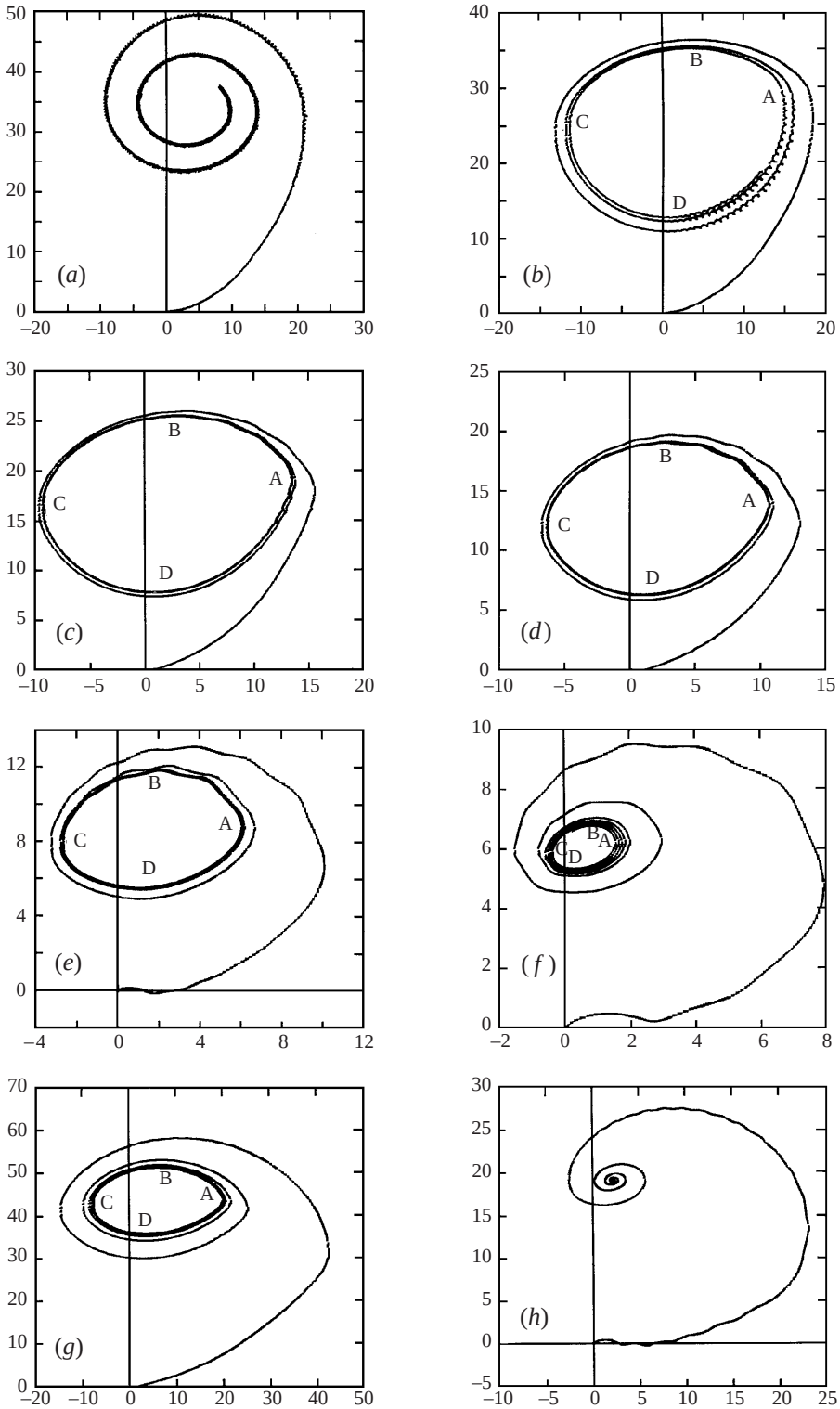

FIGURE 8. For caption see facing page.

(assuming uniform circulation), like the current velocity, by virtue of (5), the oscillatory lift force will increase in proportion to the cylinder velocity, and thus in proportion to the distance from the pivot. This will produce a corresponding difference in the steady and oscillatory responses, compared to the two-dimensional case defined by (6) and (7). Nevertheless these and other runs reproduce qualitatively most features of the experimental response, apart from the case with $\bar{\alpha} = 0.2$ which is discussed in the following section; the differences in magnitude are not unexpected given the idealization in the computations, i.e. two-dimensional, laminar and low Reynolds number ($Re_{cur} = 200$) flow, compared with the linear-mode, transitional/turbulent and higher Reynolds number, three-dimensional flows of the experiments. A, B, C and D, corresponding to times of maximum x response, maximum y response, minimum x response and minimum y response respectively, are marked on figure 8 for $\bar{\alpha} \geqslant 0.25$ to relate to plots in the following section.

The 'instantaneous' c_L and α due to flow relative to the cylinder are of interest to determine whether quasi-steady assumptions are of value. It is well known, for example, that the flow-induced oscillation known as galloping resulting from the variation of lift with angle of incidence for non-circular sections is a quasi-steady phenomenon (see Thompson & Stewart 1986, §4.4). That is a unimodal vibration, however, whereas the present case is bimodal, which adds very considerably to the complexity of the analysis. The matter is nevertheless explored in the following section, where it is shown that the relation between instantaneous c_L and α is not a quasi-static one (there being a marked hysteresis loop). The gradient is generally negative, which is analogous to the requirement for galloping in the quasi-static unimodal case, despite the much greater complexity of the stability problem.

6. Computed flow and force characteristics

Instantaneous lift and drag coefficients and α are based on the relative onset velocities: $u_{rel} = U_{cur} - \dot{x}, v_{rel} = -\dot{y}$, so that the angle of incidence $\theta = \tan^{-1}(v_{rel}/u_{rel})$ and velocity magnitude $U = \sqrt{u_{rel}^2 + v_{rel}^2}$, gives an instantaneous $\alpha = U/U_{rot}$. If the x, y forces are denoted by F_x, F_y then the corresponding lift and drag forces transverse to and in line with the instantaneous onset velocity are given by

$$F_L = F_y \cos(\theta) - F_x \sin(\theta),$$

$$F_D = F_x \cos(\theta) + F_y \sin(\theta).$$

Lift is then normalized so that instantaneous $c_L = F_L/(\rho U \Gamma)$ and c_D (as distinct from C_D) is normalized in the same way for comparison with c_L.

First the variations of x and y response with time are shown in figure 9 for the eight cases of figure 8 (with $\bar{\alpha} \geqslant 0.15$). Points A, B, C and D relate to those on figure 8. The cylinder axis is fixed in position up to time $tU_{rot}/D = 5$, before release.

A typical example of force variation with time for periodic oscillation with $\bar{\alpha} \gtrsim 0.25$ is shown in figure 10 for $V_r = 14$ and $\bar{\alpha} = 0.4$. Figure 10(a) shows the x and y force variation with time and figure 10(b) the variations of c_L, c_D and α with time. Points A, B, C, D on figure 10(a) coincide with maximum x force, maximum y force, minimum

FIGURE 8. Variations of computed y response with x, both normalized by D: (a) $\bar{\alpha} = 0.15$ and $V_r = 14$. (b) $\bar{\alpha} = 0.2$ and $V_r = 14$. (c) $\bar{\alpha} = 0.25$ and $V_r = 14$. (d) $\bar{\alpha} = 0.3$ and $V_r = 14$. (e) $\bar{\alpha} = 0.4$ and $V_r = 14$. (f) $\bar{\alpha} = 0.5$ and $V_r = 14$. (g) $\bar{\alpha} = 0.3$ and $V_r = 25$. (h) $\bar{\alpha} = 0.5$ and $V_r = 25$.

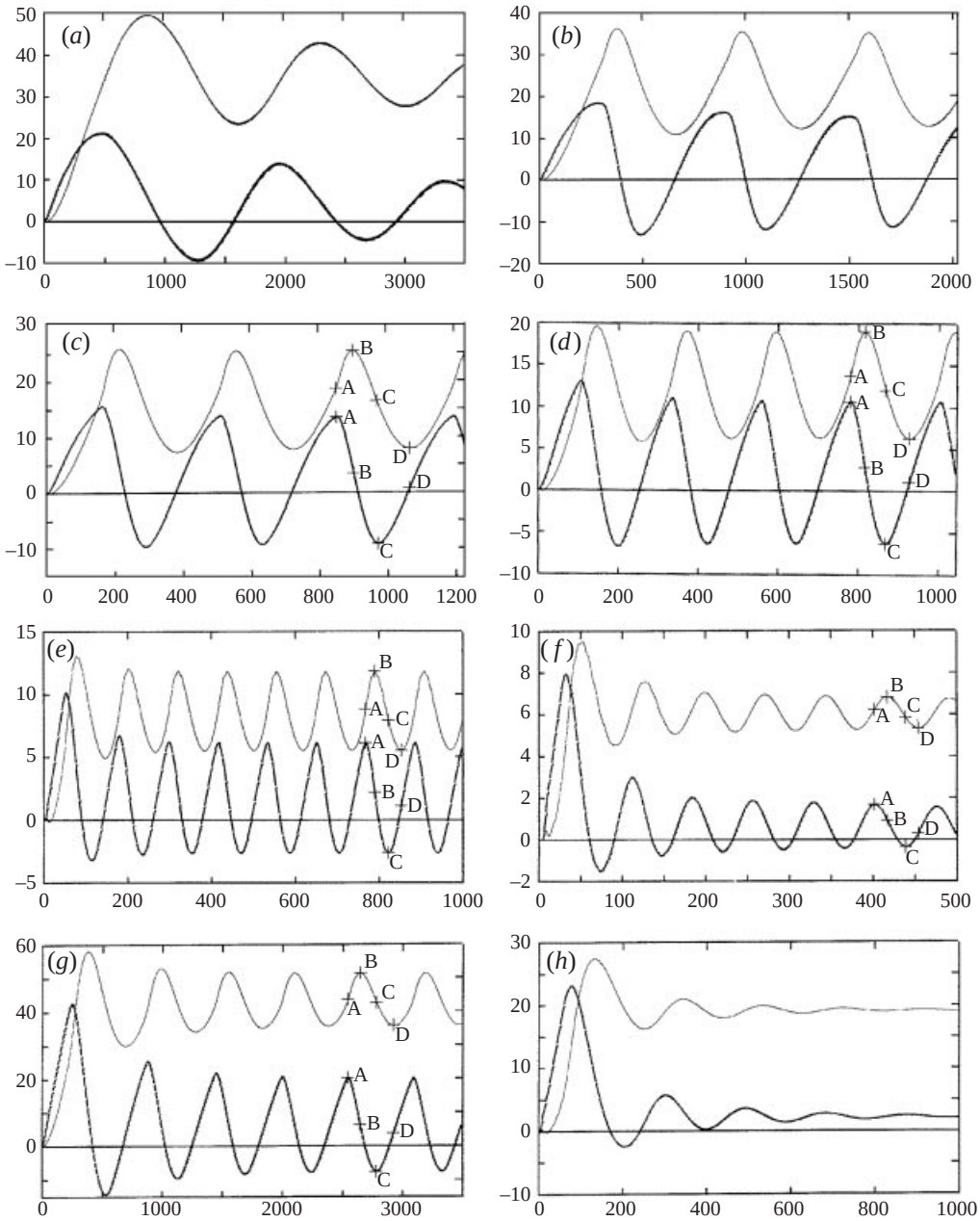

FIGURE 9. Variation of y/D (upper curve) and x/D (lower curve) with (tU_{rot}/D). $\bar{\alpha}$ and V_r values as figure 8.

x force and minimum y force respectively corresponding to maximum x response, maximum y response, minimum x response and minimum y response in figure 9(e). Points A, B, C, D are also marked on figure 10(b) and do not coincide with maximum and minimum c_L (which is based on flow relative to the cylinder).

From figure 10(b) it is clear that a rapid increase in α around time A coincides with a rapid decrease in c_L. Streamline and vorticity patterns (for flow relative to

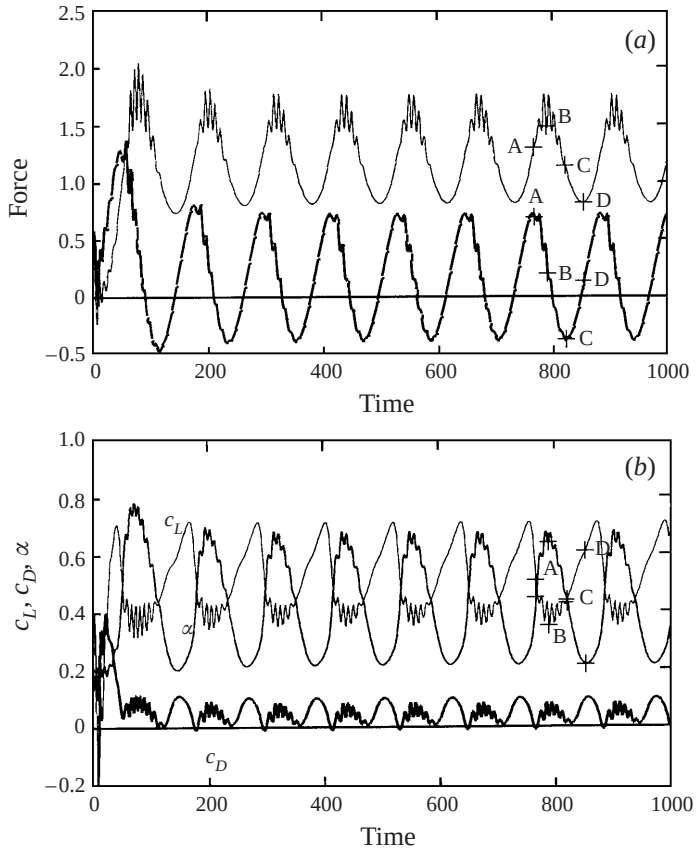

FIGURE 10. Variations of (*a*) x and y forces (lower and upper curves respectively) and (*b*) instantaneous c_L, c_D and α with time (tU_{rot}/D) for $\bar{\alpha} = 0.4$ and $V_r = 14.0$. Force is normalized by $\rho U_{rot}^2 D/2$.

the cylinder) are shown in figure 11 for times $tU_{rot}/D = 370$, 405, 410, 420, 425, 430, 435 and 475. For the first two times with 'small' α, corresponding to position D, the stagnation point is well below the cylinder, typical of a non-responding cylinder with $\alpha < 0.25$. As α increases rapidly the stagnation point moves upwards towards the cylinder and an attached wake starts to form at about time 410. By time 420 a wake has formed corresponding with position A. This is associated with a marked decrease in c_L. With high α around position B the attached wake fluctuates rapidly about some slowly varying position and this is responsible for the high-frequency components in the force variation, the period being about $10D/U_{rot}$. By time 475, corresponding with position C, the wake is about to collapse and the stagnation point moves away from the cylinder as the cycle is completed.

Plots of c_L against α are shown in figure 12 (except for $\bar{\alpha} = 0.15$ and 0.2) with positions A, B, C and D marked. These are plotted for the second half of the time series where the motion has become periodic for all cases except that with $\bar{\alpha} = 0.5$. It can be seen that the gradient is generally negative and the periodic dynamic response is associated with a pronounced hysteresis loop. It is interesting to see that the high-frequency behaviour is quite repeatable from one cycle to another. The c_L vs. α curves

(*a*)

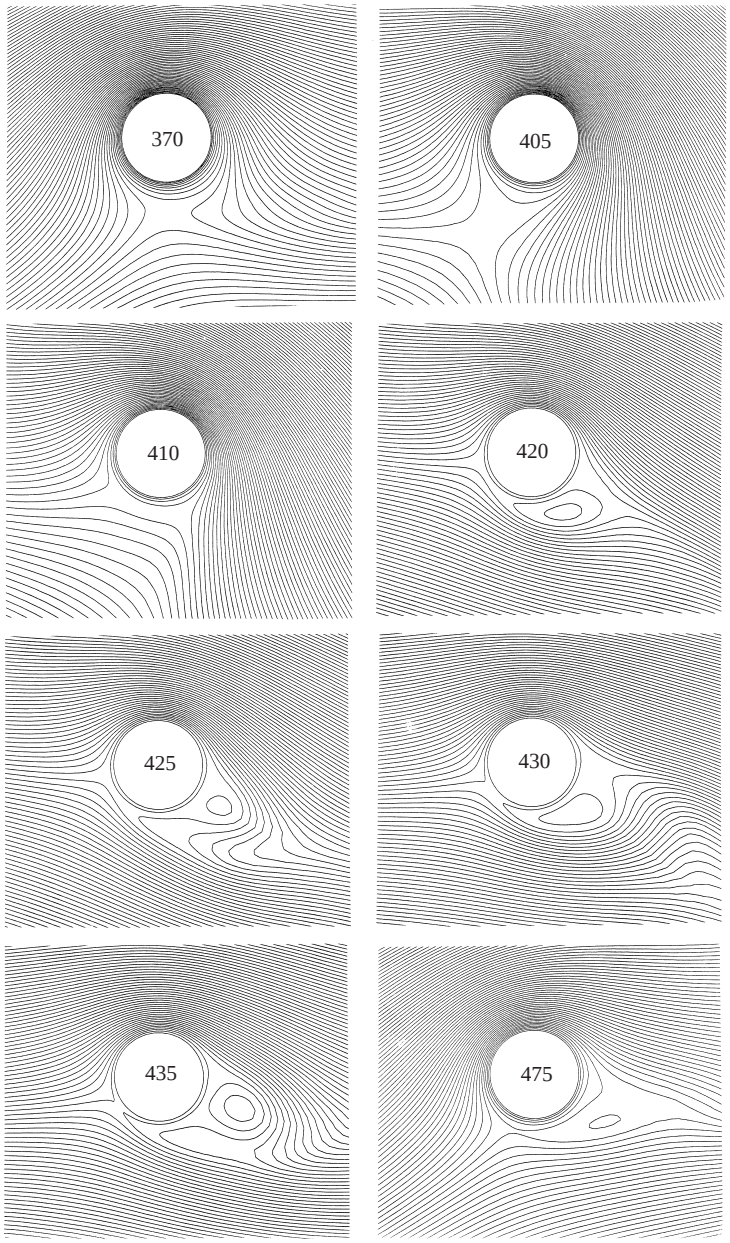

FIGURE 11 (*a*). For caption see facing page.

effectively define the response since c_D is very small in relation to c_L. Unfortunately the curves are quite complex and different for each case. The variation of c_L with α in a cycle is thus far removed from that for a non-responding cylinder with a hysteresis loop which becomes more pronounced as the dynamic response becomes bigger.

The cases with $\bar{\alpha} \leqslant 0.2$ are now considered. For $\bar{\alpha} = 0.2$ the periodic dynamic response in figure 8(*b*) shows high-frequency components superimposed on the slowly varying oscillation. This is in contrast to the experiments at this $\bar{\alpha}$ which show negligible large-amplitude dynamic response. Variations of force with time are plotted

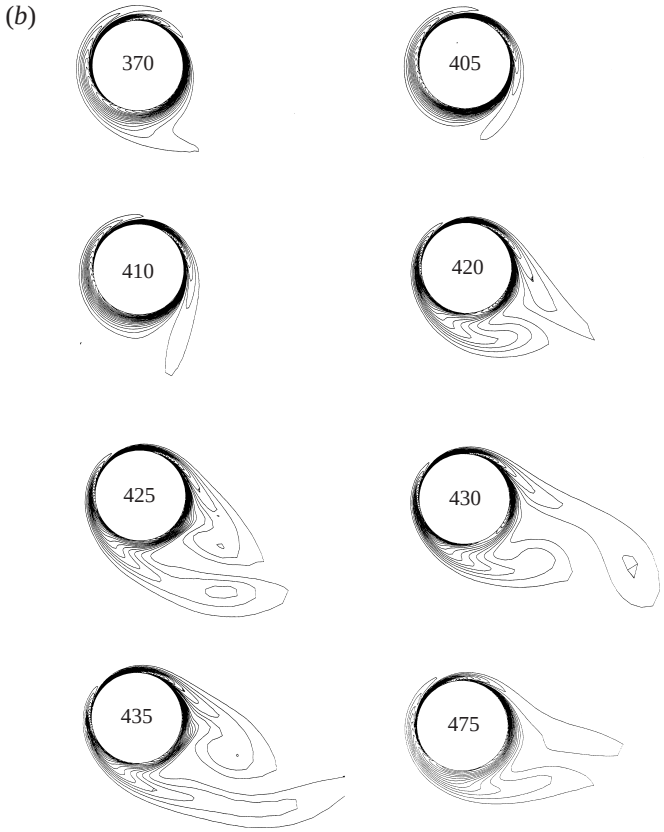

FIGURE 11. (*a*) Streamline and (*b*) vorticity plots for $\bar{\alpha} = 0.4$ and $V_r = 14.0$ at $tU_{rot}/D = 370$, 405, 410, 420, 425, 430, 435, 475 (as marked on the figure). The flow is relative to the cylinder.

in figure 13 showing marked high-frequency components. The variations of instantaneous c_L and α with time are very spikey as the velocity relative to the cylinder can be very small; presenting these parameters is not of value. An example of the nature of the flow (relative to the cylinder) in a high-frequency region is shown in the streamline and vorticity plots in figure 14 where the stagnation point circulates around the cylinder and at one point disappears as the relative velocity is almost zero. The vorticity close to the cylinder shows attached coherent structures developing and collapsing. With $\bar{\alpha} = 0.15$ the large-amplitude dynamic response shown in figure 8(*a*) is clearly decaying to a steady position, as in the experiments. A high-frequency, low-amplitude dynamic response is however still apparent. A high-frequency response was also observed in the experiments although at the time it was thought to be a result of slight misalignment of the rotation mechanism as a hydrodynamic cause was considered unlikely. The small-scale vorticity structures which are formed interact with the high-frequency response which could in turn feed the low-frequency, high-amplitude response. However in the experiments, response was, negligible for $\bar{\alpha} < 0.25$ and this could be because three-dimensional and turbulence effects at much higher Reynolds numbers destroy the small-scale vorticity structures.

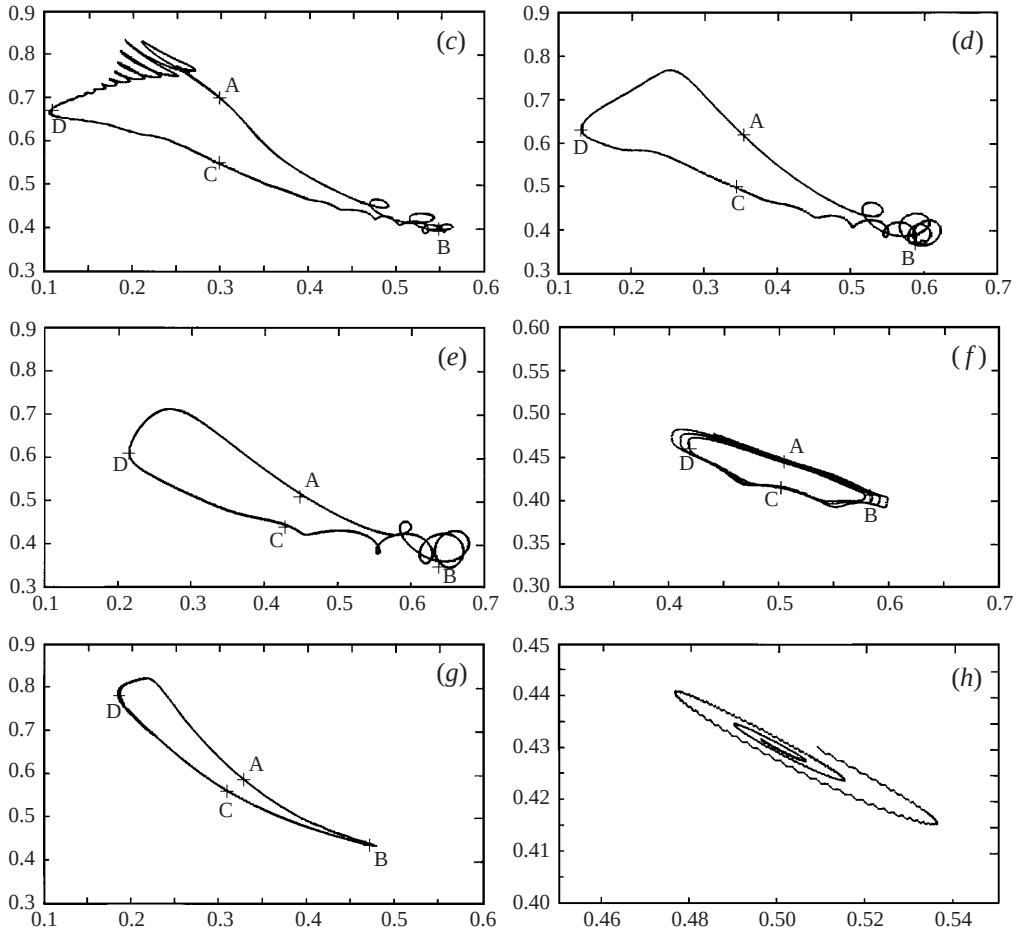

FIGURE 12. Plots of instantaneous c_L against α. $\bar{\alpha}$ and V_r values as figure 8.

The case with $V_r = 5.2$ and $\bar{\alpha} = 0.3$ was also computed to determine whether dynamic response decreases as V_r is reduced as in the experiments. Peak-to-peak responses of about $2D$ in the x- and y-directions occurred and the c_L vs. α curve still showed a hysteresis loop. Thus the response (static as well as dynamic) becomes smaller as V_r is reduced, but it has not become as small as in the experiments, where it is negligible for $\bar{\alpha} = 0.3$ although it picks up at $\bar{\alpha} \sim 0.4$.

It should be mentioned that these computations are extremely time-consuming. The high-frequency flow structures need to be resolved, requiring a small time step, while the slow oscillations require long times to cover several cycles. The above runs required 4/5 days of computation time (each) on a modern workstation (Dec Alpha 600). The mesh with 80×80 cells was generally used with a time step given by $\Delta t U_{rot}/D = 0.05$. While such a complete Navier–Stokes solution is necessary with wake formation (for $\bar{\alpha} \gtrsim 0.25$), for small $\bar{\alpha}$ a method based on matched asymptotic expansions would be highly efficient and worth investigating.

In this study we have been concerned with dynamic (and static) response for constant rotation. It is clear that with impulsively started rotation large dynamic

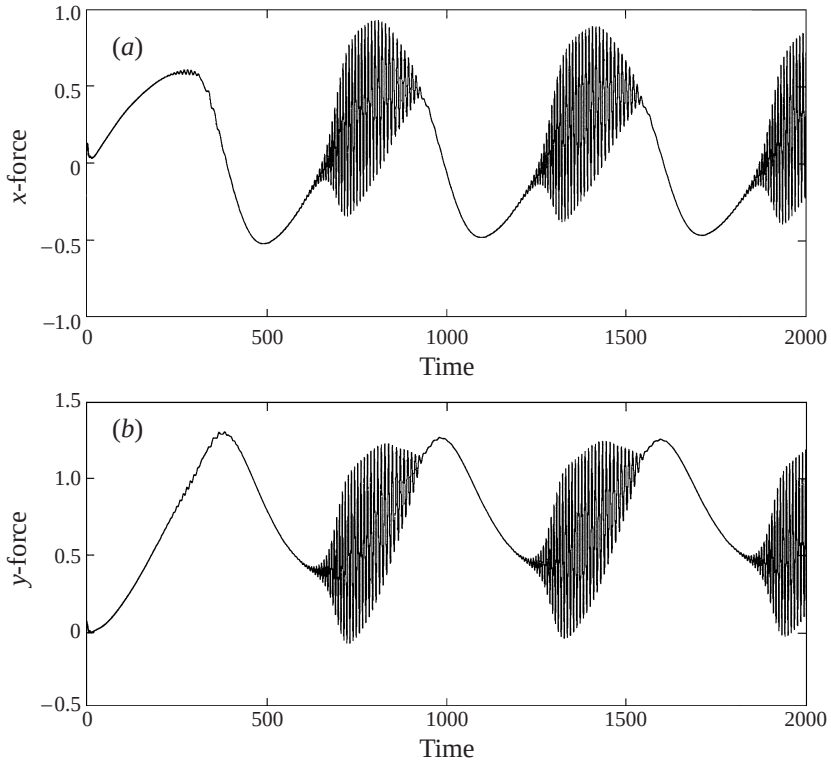

FIGURE 13. Variations of x and y forces with time (tU_{rot}/D) for $\bar{\alpha} = 0.2$ and $V_r = 14.0$. Force is normalized by $\rho U_{rot}^2 D/2$.

response generally occurs initially even when it eventually decays. Changes in rotation speed which are not impulsive may also produce significant dynamic response. This merits further investigation.

7. Conclusions

Some simple experiments have revealed a new form of orbital response for a rotating cylinder in a current for $0.25 < \bar{\alpha} < 0.5$. The cylinder undergoes orbital motion with a frequency much lower than the structural natural frequency. A two-dimensional computational study shows how rapid changes in lift coefficient c_L are associated with rapid movement of the stagnation point towards the cylinder surface, causing wake formation. This eventually ceases and the stagnation point moves away from the surface, completing the cycle. The flow is far from quasi-steady with a pronounced hysteresis loop in the cyclic variation of c_L with α when dynamic response occurs. Small-amplitude orbital motion can co-exist with low-frequency, high-amplitude orbits, the orbits having opposite rotation, and is most marked for $\bar{\alpha} \lesssim 0.25$. This phenomenon is consistent with a simple potential-flow idealization of lift behaviour. The computed response at $\bar{\alpha} = 0.2$ associated with attached boundary-layer structures was not observed in the experiments; this difference could be due to turbulence and three-dimensional effects in the experiments destroying the small-scale structures.

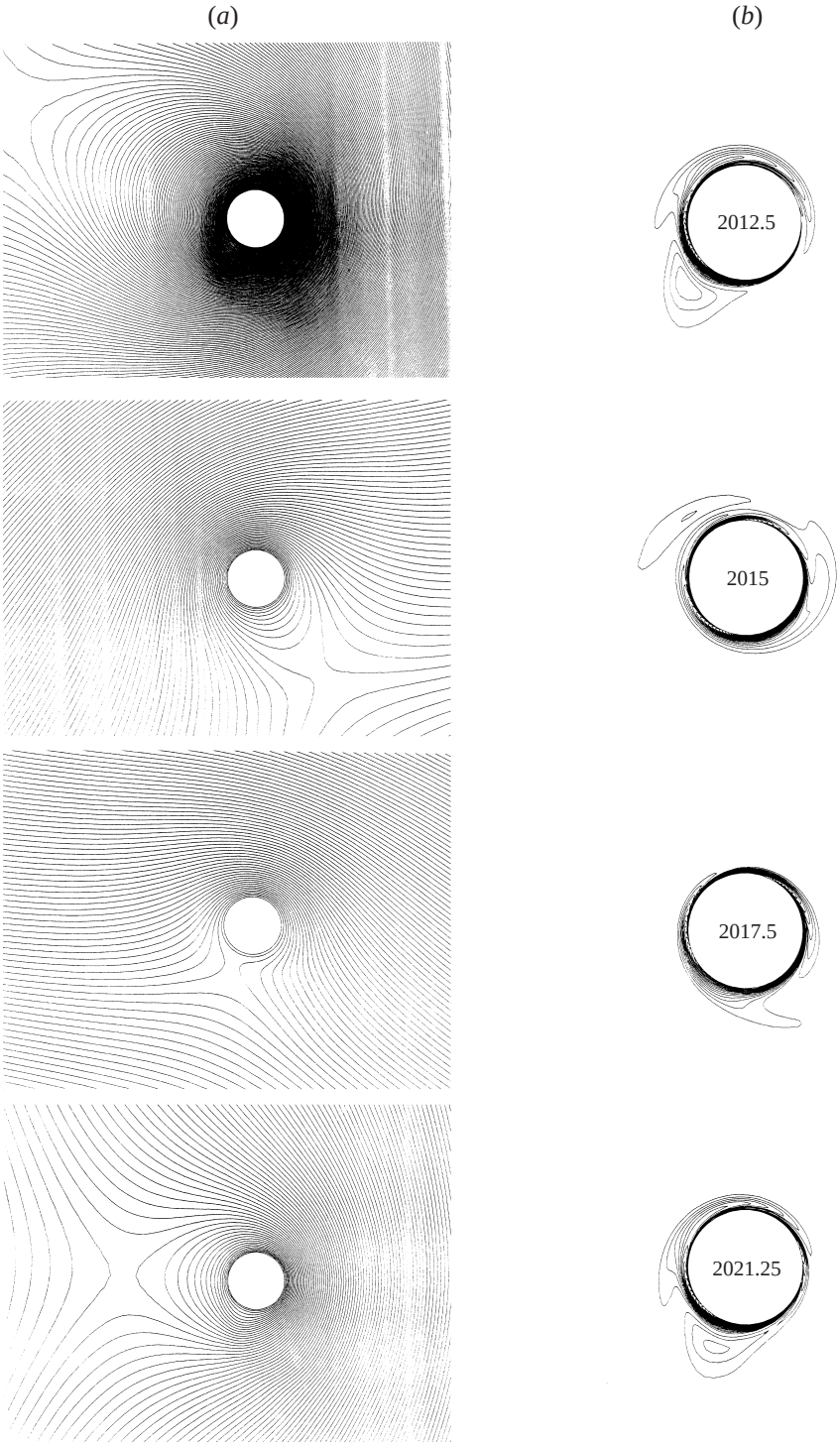

FIGURE 14. (*a*) Streamline and (*b*) vorticity plots for $\bar{\alpha} = 0.2$ and $V_r = 14.0$ at $tU_{rot}/D = 2012.5$, 2015, 2017.5, 2021.25 (as marked on the figure). The flow is relative to the cylinder.

This work was supported on a contract for Conoco (US) while the first author was at the Victoria University of Manchester. Dr D. Chen assisted in the experimental work and undertook the video analysis. The experiments were made in a flume at Imperial College with help provided by the Department of Civil Engineering there. Consideration of gyroscopic effects was suggested by a referee. All are gratefully acknowledged.

Appendix. Gyroscopic effects

Since the cylinder in the experiments is orbiting about a pivot, like an inverted top, it is in principle necessary to consider gyroscopic effects. Consider first the case when this effect should be zero, which is when the cylinder is not rotating, but is merely orbiting as shown in figure 1(*a*), with an angular speed Ω. Its angular velocity then has no component along the cylinder axis, but merely a normal component $\Omega \sin\theta$, where θ is the inclination of the cylinder from the vertical. Its angular momentum about the pivot is thus $I\Omega \sin\theta$ in the same direction, where I is the moment of inertia in that direction, again about the pivot. For small θ the rate of change of this angular momentum is $I\Omega^2\theta$. Since $I = mL^3/3$ (where L is the length of the cylinder and m its mass per unit length) this rate of change of angular momentum is equal, as it should be, to the moment about the pivot of the centrifugal force shown in figure 1. This force varies along the cylinder and totals $mL^2\Omega^2\theta/2$, acting at a point $2L/3$ from the pivot.

In § 2 the two-dimensional hydrodynamic added mass is included in m; the same applies to the present case as shown in Rainey (1995), where the modification to this two-dimensional added mass term due to angular velocity is show to vanish provided the axial water velocity along the cylinder is zero (see Rainey 1995 equations (1) and (3)), as it is here. Hence $m = (1+\beta)\rho\pi D^2/4$, as in § 2.

Consider now the case when the cylinder is rotating, with angular velocity ω, as shown in figure 1(*b*), thereby introducing a gyroscopic effect. It will now have an additional angular momentum $I'\omega$, where I' is the moment of inertia of the cylinder about its axis, which clearly has no hydrodynamic component and is thus $L\beta\rho\pi D^4/32$. For small θ, the rate of change of angular momentum is $-I'\omega\Omega\theta$, so in total the rate of change of angular momentum is $I\Omega^2\theta(1-(I'/I)(\omega/\Omega))$. Thus the gyroscopic effect is equivalent to modifying the centrifugal force in figure 1 by a factor

$$(1-(I'/I)(\omega/\Omega)) = (1-(3/8)(D/L)^2(\beta/[1+\beta])(\omega/\Omega))$$

In § 2, this factor will be applied to m and thus to the existing multiplier $(1+\beta)$ in equations (2)–(4). It is therefore also the correction factor to the frequency ratio in (4) and thus approximately equal to the correction factor to the ratio T/T_o plotted in figure 7.

Numerically, D/L is at most 0.025, $\beta/(1+\beta) = 0.73$, and $-\omega/\Omega$ is at most 70 (when $D/L = 0.025$), so the correction factor is $(1+0.012)$ or 1.2%. Thus the experimental results in this paper do not require significant correction for gyroscopic effects.

REFERENCES

Batchelor, G. K. 1967 *An Introduction to Fluid Dynamics*. Cambridge University Press.

Betz, A. 1925 *Z. Ver. deutsch. Ing.* **69**, 11–14.

Bishop, R. E. D. 1959 The vibration of rotating shafts. *J. Mech. Engng Sci.* **1**, 50–65.

Chew, Y. T., Cheng, M. & Luo, S. C. 1995 A numerical study of flow past a rotating circular cylinder using a hybrid vortex scheme. *J. Fluid Mech.* **299**, 35–71.

Clough, R. W. & Penzien, J. 1975 *Dynamics of Structures*. McGraw-Hill.

Govardhan, R. & Williamson, C. H. K. 2000 Modes of vortex formation and frequency response of a freely vibrating cylinder. *J. Fluid Mech.* **420**, 85–130.

Karniadakis, G. E. & Triantifyllou, G. S. 1992 Three-dimensional dynamics and transition to turbulence in the wake of bluff objects. *J. Fluid Mech.* **238**, 1–31.

Keulegan, G. H. & Carpenter, L. H. 1958 Forces on cylinders and plates in an oscillating fluid. *J. Res. Natl Bur. Stand.* **60**, 423–440.

Lien, F. S. & Leschziner, M. A. 1994 A general non-orthogonal finite-volume algorithm for turbulent flows at all speeds incorporating second-moment closure, Part 1 Numerical implementation. *Comput. Meth. Appl. Mech. Engng* **114**, 123–148.

Milne-Thomson, L. M. 1968 *Theoretical Hydrodynamics*, 5th Edn. Macmillan.

Moore, D. W. 1957 The flow past a rapidly rotating circular cylinder in a uniform stream. *J. Fluid Mech.* **2**, 541–550.

Prandtl, L. & Tietjens, O. G. 1934 *Applied Hydro- and Aeromechanics*. McGraw-Hill.

Rainey, R. C. T. 1995 Slender-body expressions for the wave loads on offshore structures. *Proc. R. Soc. Lond.* A **450**, 391–416.

Smith, P. A. & Stansby, P. K. 1988 Impulsively started flow around a circular cylinder by the vortex method. *J. Fluid Mech.* **194**, 45–77.

Thompson, J. M. T. 1982 *Instabilities and Catastrophes in Science and Engineering*. Wiley.

Thompson, J. M. T. & Stewart, H. B. 1986 *Nonlinear Dynamics and Chaos*. Wiley.